Microwave-Assisted Synthesis of Porous Composites MOF–Textile for the Protection against Chemical and Nuclear Hazards

Nelly Couzon, Manuela Ferreira, Sylvain Duval, Ahmida El Achari, Christine Campagne, Thierry Loiseau, Christophe Volkringer

Microwave-assisted Synthesis of Porous Composites MOF-Textile for the Protection against Chemical and Nuclear Hazards

*Nelly Couzon[a], Manuela Ferreira[b], Sylvain Duval[a], Ahmida El-Achari[b], Christine Campagne[b], Thierry Loiseau[a], Christophe Volkringer[a] **

[a] Univ. Lille, CNRS, Centrale Lille, UMR 8181 – UCCS – Unité de Catalyse et Chimie du Solide, F-59000 Lille, France.

[b] Univ. Lille, ENSAIT, ULR 2461 – GEMTEX – Génie et Matériaux Textiles, F-59000 Lille, France

KEYWORDS: UiO-66, microwave-assisted synthesis, abrasion, textiles, DMNP degradation, radioactive species sorption

HIGHLIGHTS

- Assisted-microwave process of UiO-66/UiO-66-NH_2 deposition on textiles
- Performing normed abrasion resistance measurement
- Protection against several chemical and nuclear hazards

ABSTRACT

Since the emergence of CBRN (Chemical, Biological, Radiological and Nuclear) risks, significant efforts have been made to create efficient personal protective equipment. Recently, Metal-Organic Framework (MOF) materials have emerged as new promising candidates for the capture and degradation of various threats, like Chemical Warfare Agents (CWAs) or radioactive species. Herein, we report a new synthesis method of MOF-textile composite by microwave irradiation, with a direct anchoring of MOF on textiles. The resistance of the composite has been tested using normed abrasion measurements and non-stable samples were optimized. The protective capacity of the MOF/textile composite have been tested against dimethyl 4-nitrophenyl phosphate (DMNP), a common CWA simulant, showing short degradation half-life (30 min). Radiological/nuclear protection has also been tested, through a uranium uptake (up to 15 mg. g^{-1} of adsorbent) and the capture of Kr or Xe gas, with 0.9 and 2.9 cm^3/g, respectively.

INTRODUCTION

Chemical, biological, radiological and nuclear (CBRN) weapons are one of the most serious threats of this century. It gathers any substances that can be deliberately used to harm or kill people, whether by accident or intentional release on civilians or military.[1] Within the class of CBRN threats, one can find chemical warfare agents (CWAs) such as nerve agents (Tabun, Soman, VX, …) or mustard gas, as well as biological hazards (anthrax, botulism toxin, ricin toxin, …) or radioactive elements like actinides (e.g. uranium, plutonium) or polonium.[2] Against these various risks, several specific protective equipments have to be designed to respond to any situation, as no unique protective clothing can be efficient against all the possible dangers. The type and the nature of required protection depend on the toxic substance (chemical or radiological, liquid or gas), the conditions and time of exposure. Protection of respiratory track is generally the first priority and is provided by gas mask containing activated carbon absorbents, sometimes impregnated with metallic salts (mainly Cu, Ag, Zn or Mo), which act as active adsorption sites to enhance the capture efficiency.[2] For the protection of the entire body, cloths are expected to provide not only a barrier to toxic compounds but also to be durable, resistant, air and water vapor permeable and comfortable.[3,4] For these needs, the use of permeable protective clothing have been largely developed using porous materials as absorbent.[5–7] Indeed, this class of compounds presents high surface area (several hundred of m^2/g) which increase the possible contact with the toxic species and act as a filter to CBRN threats. Depending on the hazard targeted, the pore sizes can be adapted, from macroporous (>50 nm) to microporous (< 2 nm). For example, microporous solids are well adapted to capture molecular CWAs whose sizes are generally close to 6-7 Å.[8]

The most used absorbent nowadays is activated carbon, which can be encountered in various shapes like granular, pellets or fibers.[6] Others absorbents such as zeolites, mesoporous metal oxides, aerogels or Metal-Organic Frameworks (MOFs) have been studied.[9–13] MOF materials have attracted much attention lately due to its dual capacity to adsorb and detoxify CWAs.[14–17] Screening tests on large variety of MOF candidates highlighted the excellent results of zirconium-based compounds such as the UiO-n (UiO : University of Oslo) family, MOF-808, PCN-222 or NU-1000 (NU: Northwestern University) against CWAs, due to the inherent Lewis acidity of the zirconium metal nodes.[18–22] Furthermore, tailoring the pore sizes, the organic linker functional groups or the zirconium-containing node connectivity have a great influence on the catalytic activity of the MOF solid.[16,23,24] For example, the decontamination of dimethyl 4-nitrophenyl phosphate (also called paraoxon-methyl or DMNP), a common nerve agent simulant, have been tested with powdered UiO-66, UiO-66-NH_2 and UiO-67, giving respectively half-life of 22, 2.8 and 7.7 min.[25] The node connectivity has also a high influence, as MOF-808 have shown one of the best degradation results for DMNP thank to its highly accessible Zr_6-based clusters.[26]

For applications in personal protective garments, MOF solids were also integrated to fabrics. Their direct deposition is possible by using classical synthesis methods such as hydrothermal or a layer-by-layer routes.[27,28] However, problems of anchoring and/or homogeneity of the MOF coating on the surface of the textile fiber have often been reported.[28,29] To overcome these issues, several strategies have been developed.[29] Among them, electrospinning have been largely investigated, and allowed the generation of a polymeric fiber enclosing the MOF or its precursors, bypassing its difficult anchoring.[30] Nevertheless, the problem of MOF accessibility has been mentioned and this technique cannot be applied to woven fabrics. Another way is the fiber or MOF

functionalization, in order to facilitate the interaction between the fiber and the porous MOF crystallites. For natural fibers, despite the presence of numerous surface groups functionalities (e.g. hydroxyl, carboxyl), specific post-treatment such as mercerization or carboxymethylation are common to enhance the anchoring and the homogeneity of the MOF coating.[31,32] Since synthetic fibers surfaces are more inert, the addition of polydopamine (PDA) or an oxide layer (TiO_2, Al_2O_3 or ZnO) by Atomic Layer Deposition (ALD) are more adapted, leading to excellent results.[33–35] Another approach is the post-synthetic modification (PSM) of the organic linker from a MOF solid with highly reactive chemical groups. In Kalaj and Cohen work,[36] the amine function of UiO-66-NH_2 was transformed into an isothiocyanate group. Combined with polythiourea, an uniform coverage of such modified UiO-66 compound has been observed on a Nyco fabric (blend of nylon and cotton) with a good adhesion.[36] Whereas the homogeneous deposition of MOFs at the surface of within the textiles fibers is well proved, the resistance of the composite and the mechanical strength of the anchored MOF is very rarely studied with normed techniques.[36,37]

Herein, we report a new rapid method to coat two distinct types of textile fibers (cotton and polyamide – PA) by UiO-66 or UiO-66-NH_2, using a microwave-assisted synthesis route. This method is quite scarce for the deposition of MOF on textiles, with only a few examples describing the utilization of MIL-47, ZIF-8 or MIL-88B(Fe).[38,39] Furthermore, microwave-assisted synthesis presents the significant advantage of being time and energy saving compared to classical hydro(solvo)thermal method.[40] Moreover, this technique allows the production of monodispersed nano-crystallized particles, which are more resistant to abrasion thanks to their small size. Due to the importance of the mechanical strength of the composite textile-MOF for application as protective suit, norm-referenced abrasion tests have been carried out to verify the good anchoring

of the MOFs and the mechanical resistance of the composite. Resistant composites have therefore been tested against chemical hazard, i.e CWA simulant (DMNP) or radiological hazards as gas (Kr, Xe) or in solution ($[UO_2]^{2+}$). Indeed, ^{127}Xe and ^{85}Kr are known radiotoxic isotopes gases, which can be released in the geosphere, in case of nuclear plant accident or spent nuclear fuel reprocessing.[41] Porous MOFs are known to have the capacity for the capture of these various threats.[41–45] Other gases CH_4 or CO_2 have been also been considered for benchmarking with other UiO-n based MOFs.

EXPERIMENTAL SECTION

Materials

$ZrCl_4$ (Alfa Aesar, 99.5+ %), terephthalic acid (H_2BDC, Alfa Aesar, 98+ %), 2-aminoterephthalic acid ($H_2BDC\text{-}NH_2$, Sigma Aldrich, 99 %), acetic acid (VWR Chemicals, 99-100 %), N,N-dimethylformamide (DMF, Carlo Erba Reagents, 99.9 %), N-ethylmorpholine (NEM, Alfa Aesar, 98 %), dimethyl 4-nitrophenyl phosphate (also called paraoxon-methyl or DMNP, Sigma Aldrich, < 98 %), uranyl nitrate hexahydrate ($UO_2(NO_3)_2{\cdot}6H_2O$), provided by Orano company) and ethanol (Carlo Erba Reagents, 96 %) were all purchased commercially and used without further purification. Cotton and polyamide (PA 6,6) textiles were provided by the GEMTEX team of ENSAIT (Roubaix, France).

General protocol for UiO-66 and UiO-66-NH_2 microwave-assisted synthesis on cotton

0.35 g (1.5 mmol) of $ZrCl_4$ and 0.249 g (1.5 mmol) of terephthalic acid were mixed to 11.6 mL of DMF in a 30 mL microwave tube and the solution was stirred for 15 minutes. 3.4 mL of acetic acid and 0.5 mL of H_2O were further added to the mixture. For the syntheses involving cotton, a

volume of N-ethylmorpholine (0.25 or 0.5 mL) can be added to the solution to counterbalance the acidity of the mixture. After the homogenization, a piece of cotton (5 x 5 cm^2 surface) was added in the microwave tube, which was then placed in the microwave reactor (ANTON PAAR Monowave 450) and heated at a desired temperature (80 to 120 °C) for 10 minutes with a heating ramp of 2 min (30°C/min to 50°C/min) and an agitation of 600 rpm. After cooling, the cotton fiber was rinsed thoughtfully with ethanol (~ 100 mL), cleaned in ultrasonic bath to remove non-grafted UiO-66 or UiO-66-NH_2 crystallites and then dried at room temperature. To increase the quantity of MOF deposited on cotton, all this synthetic procedure was repeated up to 7 times.

For UiO-66-NH_2 preparation, H_2BDC was replaced by H_2BDC-NH_2 (0.272 g, 1.5 mmol), otherwise the procedure followed is identical.

General protocol for UiO-66 and UiO-66-NH_2 microwave-assisted synthesis on polyamide

For UiO-66 and UiO-66-NH_2 synthesis on polyamide, the procedure is identical to the previous preparation described with the cotton sample (5 x 5 cm^2 surface), excepting the use of the N-ethylmorpholine base. The coating deposition of the UiO-66 and UiO-66-NH_2 crystallites on polyamide has been repeated from 1 to 10 times.

For convenience, samples were named UiO-66(x)/Y or UiO-66-NH_2(x)/Y, Y = C or PA being for cotton for polyamide, respectively, and x the number of repeated synthesis procedures, related to the different stages of coating deposition.

Characterization

X-Ray Diffraction (XRD). Powder XRD data was recorded on a Bruker D8 Advance A25 diffractometer with Bragg-Brentano geometry using Cu K_α radiation, from 3 ° to 50 °, with a step size of 0.02 ° and a counting time of 0.5 s/step.

Surface area determination. N_2 or Kr adsorption isotherms were obtained at 77 K using a Micromeritics ASAP2020 apparatus after outgassing the samples at 120°C under secondary vacuum (5 Pa) for several hours. The specific area was determined using the BET method in the P/P_0 range of 0.015-0.30 for N_2 and 0.065-0.2 for Kr. Due to the low specific surface area of the synthesized composite (i.e MOF + textile), the measurement was made using Kr for the composites and N_2 for the single MOF compounds.

After specific surface area measurement, the most promising composite were tested for the adsorption of other gases (Kr, Xe, CH_4, CO_2) at 293.15 K. These gases were bought at Linde Gas for Xe (Xe 4.7, purity: 99.997%) and Kr (Kr 5.0, purity: 99.9999 %) and Air Liquid for CO_2 (N45, purity: 99.995 %) and CH_4 (N55, purity: >99.9995 %). Each composite was outgassed at 120°C under secondary vacuum for at least 2h. The bath temperature (293.15 K) has been controlled by circulating water.

Scanning Electron Microscopy. SEM images of composite fibers were obtained using a Hitachi SU5000 with an acceleration voltage of 5 keV. Samples were coated with 300 to 350 Å thickness of metallic chromium. For EDX analysis, samples were coated with 200 to 250 Å thickness of carbon.

Infrared Spectroscopy. IR spectra were acquired on a Perkin-Elmer Spectrum Two spectrometer from 4000 to 400 cm^{-1} using a diamond attenuated total reflectance (ATR).

Inductively Coupled Plasma- Optical emission spectrometry. ICP-OES was used to determine MOF loading in the composite. Samples (UiO-66(x)/C, PA or UiO-66-NH_2(x)/C, PA) of 1 x 1 cm^2

dimension were weighted and digested in concentrated H_2SO_4 before diluting it at 0.5 M (V=10 mL) for the analysis. For polyamide-containing composite, solutions were centrifuged to remove polyamide residues. To ensure that no zirconium remained in the precipitate, EDX analysis were carried out on the residue and no signal of zirconium was detected.

Mass loadings (ML) of MOF on fiber were calculated using the following equation:

$$ML = C_{Zr} * \frac{0.01}{m * W_{Zr}}$$

Where C_{Zr} is the measured concentration of Zr; m, the mass of the initial composite and W_{Zr}, the mass percentage of Zr in pristine UiO-66 and UiO-66-NH_2, i.e. 32.8 % and 31.1 % respectively.

Abrasion tests. The abrasion resistance of the composite was tested using a Martindale SDL Atlas, following the norm ISO 12947-3:1999 which consists in following the weight loss after abrasion.[46] A 3.8 cm diameter sample was placed against a 14 cm diameter wool abrasive textile, with a pressure of 9 kPa, and underwent a given number (cycle) of circular frictions at a constant speed (52 cycles/min). Cycles up to 1250 has been made on cotton, with the intervals 100, 250, 500, 750 and 1000. Additional cycles (2500 and 3750) were tested on polyamide. For this study, we considered a stable (not damaged) composite having a weight loss lower or equal to 2 % after 1250 cycles for cotton, or 3750 cycles for polyamide textiles.

Degradation of Paraoxon-Methyl (DMNP). The protocol used was similar to the one previously developed by Farha *et al*.[14] A 1 x 1 cm^2 composite sample was weighed, cut in smaller pieces and dispersed in an aqueous solution of 1 mL of N-ethylmorpholine (NEM) at 0.45 M in a 2 mL vial. After 20 minutes of stirring, 4 µL (25 µmol) of DMNP ($2.5.10^{-2}$ M) was added to the solution. Conversion of DMNP was monitored by following the formation p-nitrophenoxide, a DMNP

degradation product with a typical absorbance at 407 nm, by using a UV/Visible Shimadzu UV1800 spectrometer. A 10 µL aliquot was taken at determined intervals and diluted in 5 mL of 0.45 M NEM. Concentration of p-nitrophenoxide was then calculated using the Beer-Lambert equation, the molar absorptivity coefficient ε of p-nitrophenoxide being 18330 $M^{-1}.cm^{-1}$.[25]

Uranyl cation capture. A stock solution of 100 ppm of uranyl (VI) nitrate has been prepared by dissolving 52.5 mg of $UO_2(NO_3)_2 \cdot 6H_2O$ in 250 mL of distilled water. This uranyl concentration has been selected from literature and by taking into account the low amount of MOF in composite compared to only MOF powder.[47,48] Aqueous solutions tests were prepared by adjusting the pH (at 3, 5 or 7) with 0.1 M NaOH or 0.1 M HNO_3. Samples (1x1 cm^2, ~16.2 mg for cotton, or 9.7 mg for polyamide) were put in the 10 mL solutions for the desired contact time (1 h or 4 h) under constant magnetic agitation. After removing the samples, the solutions were diluted and the concentration of U(VI) was then measured by ICP-OES. The incertitude on the ICP measurement is under 2 %. The U(VI) ion adsorption capacity q_e is obtained following equation (1):

$$q_e = \frac{(C_0 - C_e) * V}{m}$$

With C_0 being the initial concentration of U(VI), C_e the concentration at the equilibrium, V (L) the volume of the solutions and m (g) the weight of the absorbent.

RESULTS AND DISCUSSION

Composite MOF-textile synthesis and characterization

The synthesis of UiO-66 based composite was optimized targeting both high resistance to abrasion (i.e no deterioration of the textile fibers nor the MOF) and high specific surface area. For

both cotton and polyamide fibers, optimized conditions obtained with UiO-66 were then directly extended to UiO-66-NH_2.

With cotton (C)

We have evaluated the effect of various synthesis conditions (temperature, number of coating depositions, …) on the efficiency of the deposition of UiO-66 and UiO-66-NH_2 and the stability of the resulting cotton-based composite, with a high importance according to its abrasion resistance. To verify their integrity, krypton adsorption characterizations have also been carried out before and after each abrasion test.

The microwave-assisted deposition of UiO-66 on cotton have been successfully carried out from 80 to 120 °C, with well-defined PXRD patterns corresponding to the expected pure UiO-66 phase (see Fig. 1.a). The specific surface area of the UiO-66(1)/C composite varies from 5.5 m^2/g for an 80°C heating route up to 14.0 m^2/g for a 120°C heating route. The deposition of UiO-66 crystallites on the cotton fiber seems quite homogeneous at every temperature (range 80-120°C), with well-defined particles of 55 +/- 10 nm size (Fig. 1.c and d). However, abrasion resistance tests highlighted the poor mechanical strength of the UiO-66(1)/C composite synthesized at temperatures higher than 100 °C (Fig. 1.b). Indeed, for synthesis carried out at 120°C, the UiO-66(1)/C sample is destroyed after only 100 cycles of circular frictions. At 100 °C, a weigh loss of approximately 3 % (corresponding to 4 mg) is noted after 1250 cycles. Only the UiO-66(1)/C samples synthesized at 90 °C or lower, are preserved according to the abrasion resistance tests. At 90 °C, BET measurement (Kr, 77 K) indicates that the UiO-66(1)/C composite is not altered after abrasion tests (passing from 8.0 to 7.6 m^2/g), which confirms the strong anchoring of the MOF to the fiber (Table S1). The degradation of cotton at higher synthesis temperature (100-120°C) is

likely due to the acidic synthetic conditions coming from HCl *in situ* formation after $ZrCl_4$ hydrolysis, leading to cellulose deterioration and poorer mechanical strength. For these reasons, only the UiO-66(1)/C composite resulting from the synthesis at 90 °C will be discussed hereafter.

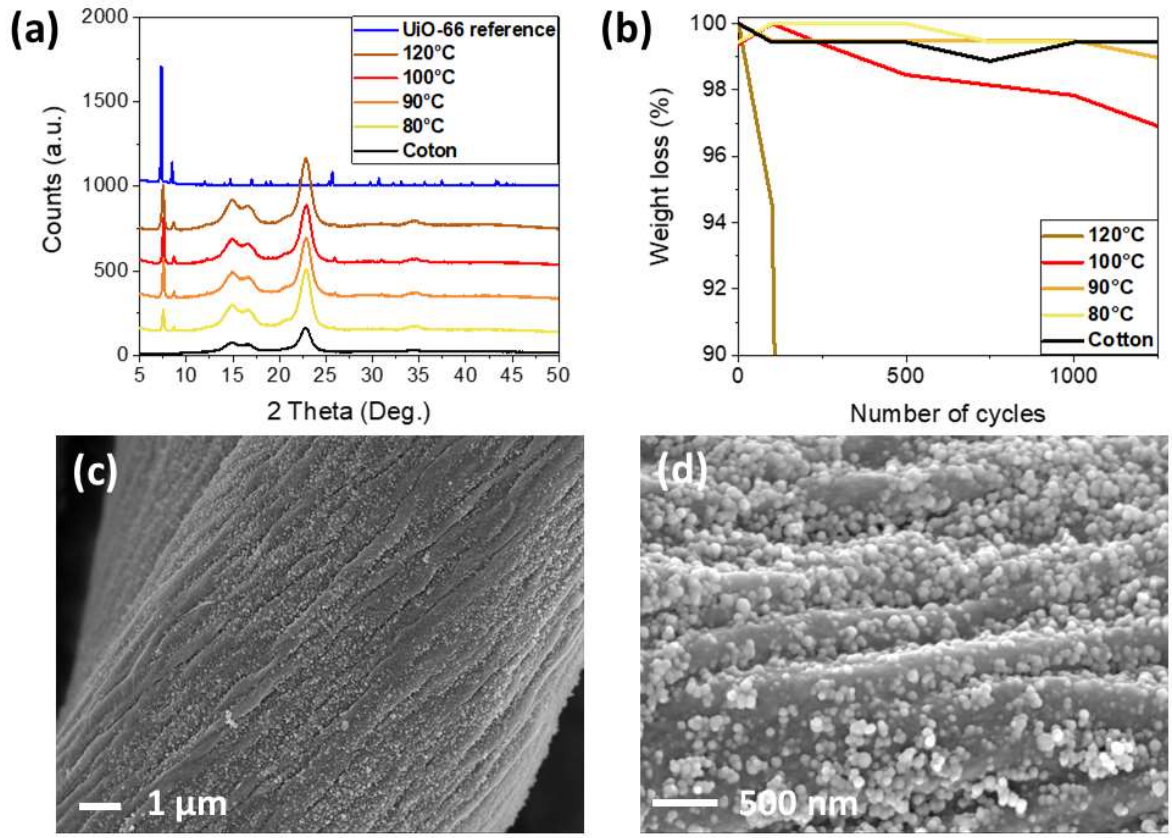

Figure 1. (a) Powder XRD patterns of UiO-66(1)/C composites synthesized at different temperatures (range 80-120°C); (b) Abrasion resistance tests of UiO-66(1)/C composites synthesized at different temperatures; (c) and (d) SEM images of UiO-66 crystallites on cotton fibers from microwave-assisted synthesis at 90 °C.

In order to increase the porosity of the UiO-66 composites, the coating deposition have been repeated several times (up to 7 coatings). As presented in Figure 2a, a linear increase of the specific surface area is observed with the increased number of UiO-66 coatings, with a maximum at 128 m^2/g after 7 times (UiO-66(7)/C sample). The evolution of deposited UiO-66 quantity is also observed by IR, with the clear visible vibration bands assigned to UiO-66 from coatings after 5 times (Fig. S1). The peaks in the 400-750 cm^{-1} region are ascribed to interactions between zirconium and the terephthalate ligand; between 661 and 746 cm^{-1}, it corresponds to the stretching vibration of $Zr\text{-}O_2$ while the peaks at 552 and 483 are assigned to the μ_3-O bond between zirconium and the organic linker. In the 1400-1700 cm^{-1} region, the band at 1398 cm^{-1} is consistent for the symmetric stretching vibration of COO, while those at 1507 and 1581 cm^{-1} are due to the stretching vibration of C=C of the phenyl rings. Finally, the 1650 cm^{-1} peak is ascribed to residual DMF trapped in the pores of UiO-66.[49,50]

The UiO-66 particles deposited on cotton fibers shows two different size distributions: 50 +/- 10 nm particles at the top of the coating related to the last deposition stages and bigger crystallites (175 +/- 25 nm) in the deeper layers from early syntheses, suggested a crystal growth process during the repetition of microwave-assisted synthesis steps (Fig. 2c and d). Nevertheless, in spite of soft conditions (90°C), such multi-coating deposition involves repeated *in situ* formation of HCl, fragilizing the cotton fiber. The UiO-66(5)/C sample (related to five UiO-66 deposition steps) is destroyed after only 100 cycles of circular frictions, but the UiO-66(3)/C sample is decomposed after a higher number of 500 cycles (Fig. 2b).

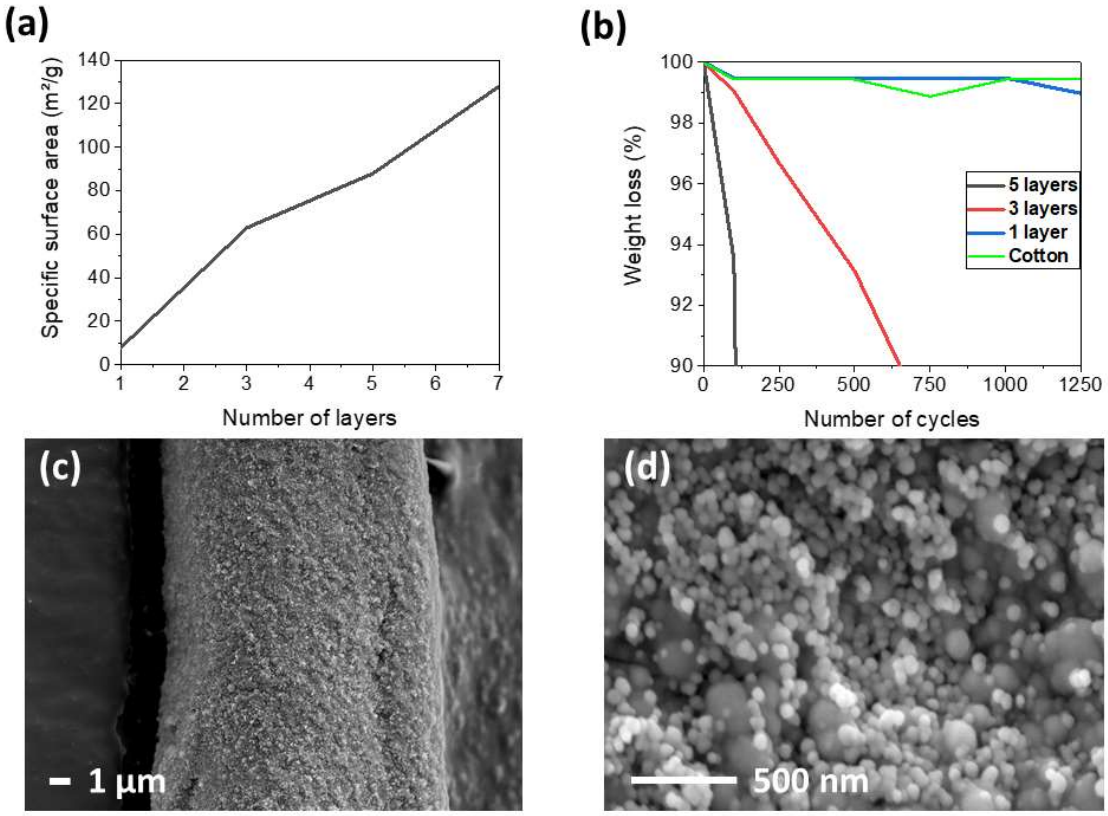

Figure 2. (a) Specific surface area in function of UiO-66 coating steps deposited on cotton (UiO-66(1-7)/C), (b) Abrasion resistance of UiO-66(x)/C samples, with x varying from 1 to 5 coating steps of UiO-66 and (c) and (d) SEM images of UiO-66(5)/C.

To limit cellulose degradation during multi-steps coating deposition caused by released HCl, N-ethylmorpholine (NEM) was added to the synthesis medium as a base agent. In addition to its basicity (pKa=7.67), this reactant is an usual co-catalyst for the degradation of organophosphorus agents.[51,52] Two different contents of NEM have been added (0.25 or 0.5 mL) to UiO-66 reaction synthesis medium, for the coating deposition numbers of 3 and 5 times. A clear enhancement of the mechanical strength of the UiO-66(3 or 5)/C composite is observed with the increasing quantity of NEM added (see Fig. S2). For the UiO-66(3)/C sample, the addition of NEM (0.25 or 0.5 mL)

leads to a stable composite even after 1250 cycles of abrasion (less than 2% weight loss). However, with the UiO-66(5)/C sample, only the addition of 0.5 mL of NEM is enough to make a stable composite. Otherwise, the addition of 0.25 mL of NEM results in more than 8% weight loss after 1250 cycles of circular frictions.

Whereas the UiO-66(5)/C composite remains stable against abrasion, the addition of 0.5 mL of NEM induces the diminution of the porosity, from 88.4 m^2/g without NEM to 47.5 m^2/g with 0.5 mL of NEM (Fig. 3.a and Table S2). This loss of porosity coincides with the XRD Bragg peaks broadening assigned to a loss of crystallinity (Fig. 3.b), as confirmed by SEM. While the addition of 0.25 mL of NEM in the reaction medium led to similar sizes and spherical forms of particles of UiO-66 than without NEM, the reaction batch with 0.5 mL of NEM gave an agglomeration of particles with no homogeneous size and a few cracks (Fig. 3.c and d). The mass loading of UiO-66 have been measured by ICP to 8.5 % and 4.1 % for the UiO-66(5)/C and UiO-66(3)/C composites, respectively. Due to its mechanical stability, the UiO-66(5)/C sample (prepared with 0.5mL of NEM) was then selected as a good compromise with a BET surface area of 47.5 m^2/g, for further DMNP degradation tests and gas capture.

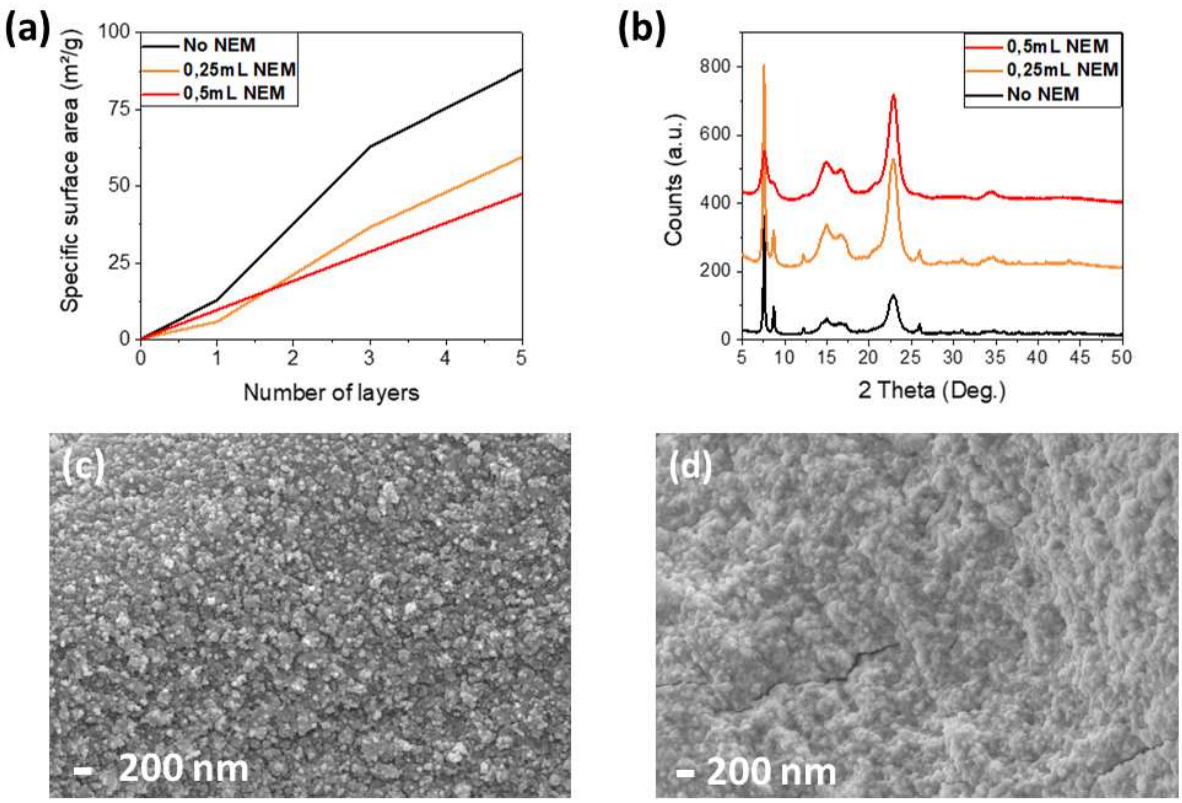

Figure 3. (a) Effect of N-ethylmorpholine (NEM) addition on the specific surface area (Kr, 77K) for UiO-66(x)/C, with x varying from 1 to 5 coating steps of UiO-66 on cotton fiber; (b) Powder XRD patterns of UiO-66(3)/C with and without NEM; (c) SEM images of UiO-66(3)/C with 0.25 mL of NEM and (d) SEM images of UiO-66(5)/C with 0.5 mL of NEM.

The protocol of the elaboration of the UiO-66(x)/C composite has been transposed to that of UiO-66-NH_2(x)/C one, which gave similar results (Fig. S3). Powder XRD patterns show the broadening of the UiO-66-NH_2 Bragg peaks when NEM is added to the reaction medium (Fig. S3. a). A good coating of the cotton fibers is observed for both UiO-66-NH_2(3)/C with 0.25 mL of NEM and UiO-66-NH_2(5)/C with 0.5 mL of NEM (Fig. S3 c and d), with mass loading of 3.7 and 7.4 % respectively, i.e slightly lower than that observed with UiO-66 (4.1 and 8.5 wt %). Specific

surface areas are close to the ones obtained with UiO-66, the UiO-66-NH_2(5)/C with 0.5 mL of NEM being at 53.3 m^2/g (instead of 47.5 m^2/g for UiO-66(5)/C, see Table S2). However, abrasion resistance was found to be much less efficient than occurring for UiO-66(5)/C, with a weigh loss of 8 % after 1250 cycles for UiO-66-NH_2(5)/C with 0.5 mL of NEM (Fig. S3. b and Table S2). However, the increase of efficiency is still notable, as without NEM the sample is destroyed after less than 500 cycles only. Even if its stability is not optimal, the UiO-66-NH_2(5)/C (prepared with 0.5 mL of NEM) sample was selected for DMNP degradation, gas and uranyl uptake.

With Polyamide (PA)

UiO-66 and UiO-66-NH_2 deposition on the surface of polyamide fabrics have been carried out with similar conditions than those used for cotton fibers. Since polyamide is stable in soft acidic conditions, the addition of a base (NEM) was not required for this fiber. UiO-66 and UiO-66-NH_2 grafting has been made at 90 °C, from 1 up to 10 coating deposition steps. At the opposite to cotton samples, the UiO-66/UiO-66-NH_2 polyamide composites are stable to abrasion, with almost no weight loss of the composite up to 3750 cycles (instead of 1250 with cotton), confirming that polyamide fibers are adapted to Zr-MOF acidic synthesis conditions (Fig. 4a). After the 3750 cycles abrasion test on the UiO-66(10)/PA composite, the specific surface area value slightly decreases from 68.7 to 63.8 m^2/g, i.e a 9 % loss, meaning that a large amount of the UiO-66 is unaffected by the friction (Table S3). The same trend (8 % loss) was observed for UiO-66-NH_2 composite.

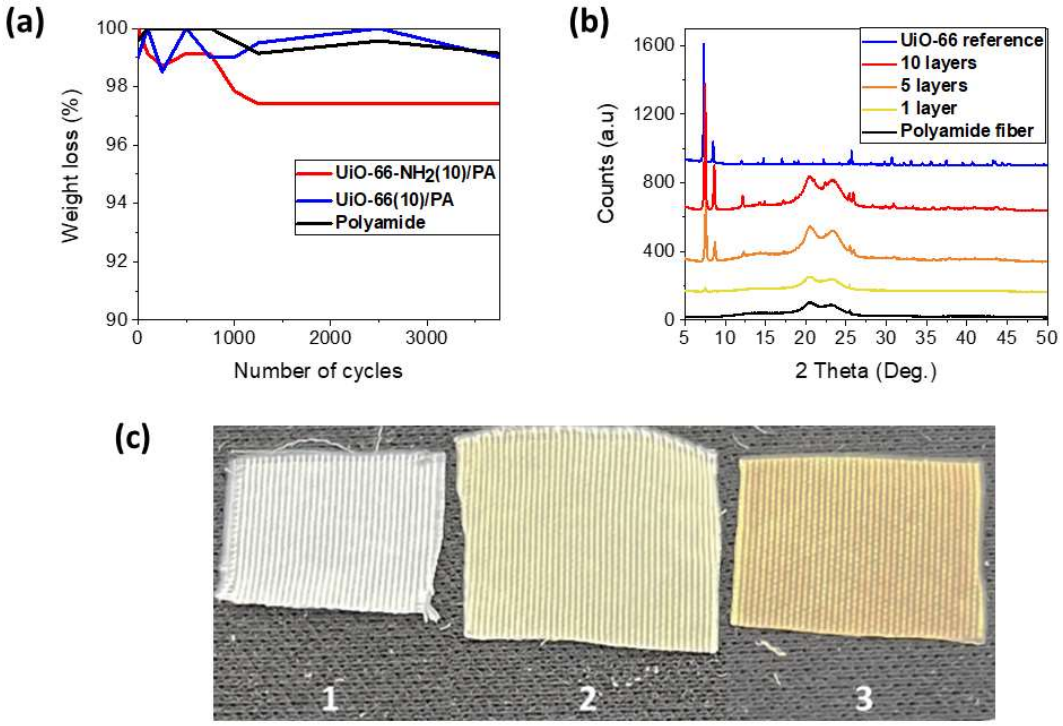

Figure 4. (a) Abrasion resistance behavior of UiO-66(10)/PA and UiO-66-NH_2(10)/PA composite on polyamide fibers and (b) Evolution of the powder XRD patterns of UiO-66(x)/PA composites as function of the number of coating depositions of UiO-66 grafted on polyamide (c) Photographs of pieces of polyamide fabrics (1) with 5 (2) and 10 (3) UiO-66-NH_2 deposition steps.

Further characterizations have therefore been carried out. The increasing quantity of UiO-66 (or UiO-66-NH_2) associated to the number of coating depositions is confirmed by different techniques (Fig. 4b and c, Fig. S4 and S5). Powder XRD patterns show the growth of the characteristic Bragg peaks at 7.5 ° and 8.6 ° (2θ) of UiO-66 from 1 to 10 coating depositions (Fig. 4b and S5a). Specific surface area increases almost linearly with the number of coating deposition stages, from 4.7 m^2/g with one stage, 37.5 m^2/g with 5 stages and 68.7 m^2/g with 10 stages for UiO-66 composite. Compared to cotton, the specific surface area is lower for the same number of coating deposition

(37.5 m²/g vs 47.5 m²/g, or even 88.4 m²/g for UiO-66(5)/C without NEM, see Table S2 and S3), highlighting that the deposition efficiency on polyamide is less favored due to the lack of numerous surface functional groups (like -OH species with cotton). For UiO-66-NH_2 deposition, a yellow-orange coloration is observed (Fig. 4c). After 10 coating deposition stages, the mass loadings determined by ICP-OES are of 6 % and 6.3 % for UiO-66-NH_2(10)/PA and UiO-66(10)/PA, respectively.

Similar to the deposition on cotton fibers, SEM observations show that the first stage of UiO-66 (or UiO-66-NH_2) deposition presents particles of 60 +/- 10 nm on the polyamide fibers. Multiples coating depositions on PA presents two particles sizes, 75 +/- 10 nm for the first coating deposition stages and 200 +/- 25 nm for the last ones (Fig. S4 and S5 b and c). Elemental EDX cartography of a cross section of a group of stacked polyamide fibers (10 times of UiO-66/UiO-66-NH_2 coating deposition) proved the homogeneous surface deposition outside the fibers (Fig. 5). Zirconium is clearly present on the edge of the fibers and an enhancement of the EDX signal for oxygen on the edge also confirms the occurrence of UiO-66 crystallites. Furthermore, cross section images allowed to determine the thickness of the deposit with 420 +/- 75 nm after five deposition stages and 700 +/- 150 nm for the ten deposition stages.

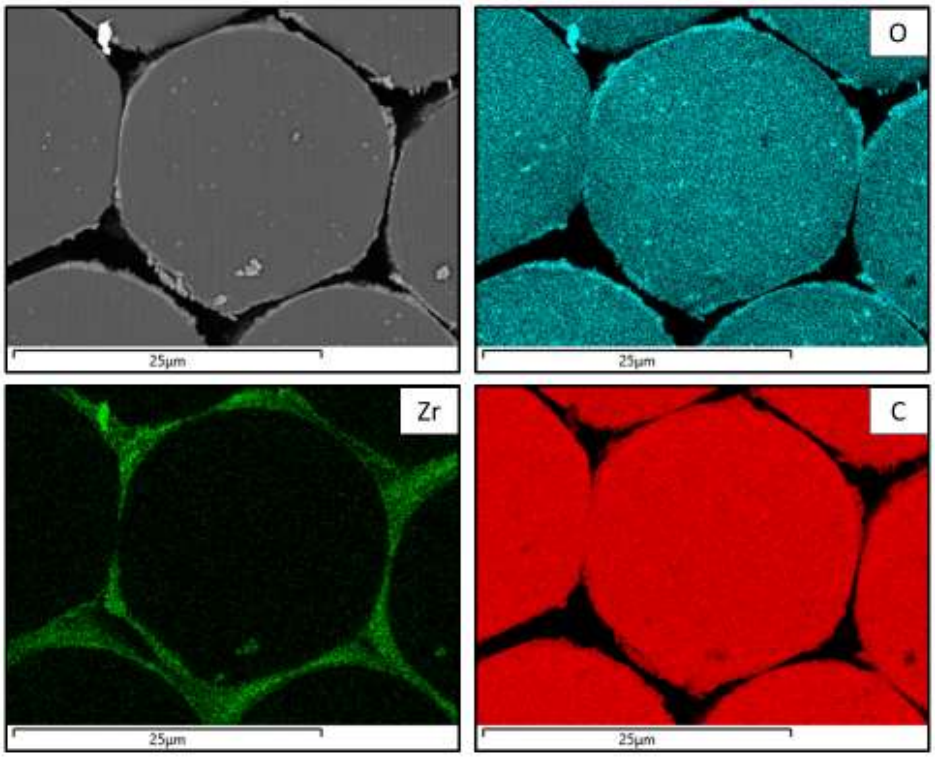

Figure 5. SEM image (top, left) and EDX elemental maps of a cross section of the UiO-66(10)/PA sample.

Applications to chemical and nuclear hazards

This study focuses on a selection of composite samples, i.e the ones possessing the best compromise between a good abrasion resistance and optimal Zr-MOF textural properties (i.e. crystallinity, specific surface). Therefore, we have chosen the following composites by using either cotton fibers, UiO-66(5)/C and /UiO-66-NH_2(5)/C products, both synthesized with N-ethylmorpholine (NEM; 0.5 mL), or polyamide fibers, UiO-66(10)/PA and UiO-66-NH_2(10)/PA products.

DMNP degradation

The UiO/cotton or UiO/polyamide composites were probed for their catalytic activity against the chemical decomposition of dimethyl 4-nitrophenyl phosphate (DMNP), a common simulant of chemical warfare agent (CWA), in aqueous solution and monitored by UV-Vis spectroscopy according to the published procedure.[14] The formation of p-nitrophenoxide species from the degradation of DMNP molecules exhibits a typical UV-Vis signature at 407 nm, which was followed periodically up to 6 h (see Fig. S6). The best half-life times of 30 min were obtained with the UiO-66-NH_2(5)/C and UiO-66-NH_2(10)/PA composites (Fig. 6). This trend can be explained by the presence of amino group which acts as a Bronsted base, facilitating the organophosphorus hydrolysis.[25] UiO-66-NH_2(5)/C shows a slightly higher activity with more than 90 % of degradation after 1h30, when UiO-66-NH_2(10)/PA degrades less than 90 % even after 6 h. This could be explained by slightly higher specific surface area and concentration values of Zr-MOF in UiO-66-NH_2(5)/C (53.3 m^2/g, 7.4 wt %), than in UiO-66-NH_2(10)/PA (33.4 m^2/g, 6 wt %).

As expected, the degradation of DMNP is slower when UiO-66-NH_2 is replaced by UiO-66.[22,53] In spite of higher specific surface of UiO-66-based composites than UiO-66-NH_2 analogues, the half-life time is multiplied by 3 and 8 for UiO-66-containing samples on cotton and polyamide, respectively (Table 1). The impact of textiles alone has been verified and very low rate of DMNP hydrolysis was noted, with approximately 7 % of degradation after 4 h for pristine cotton and pristine polyamide. However, the use of a single NEM buffer solution (0.45 M) gives rise to a value of 12 % for degradation of DMNP (after 4 h), showing that pristine cotton or pristine PA fiber slightly inhibits this efficiency. Above all, this result highlights the need of the MOF to efficiently degrade the DMNP.

Table 1. Half-life time of the DMNP hydrolysis and uranyl capture by UiO-66 and UiO-66-NH_2 composites with cotton and polyamide (PA) (DMNP: 25 µmol)

Sample	BET (SSA, m^2/g)	% wt MOF	Ratio MOF/DMNP (%)	DMNP $t_{1/2}$ (h)	Uranyl uptake q_e ($mg.\ g^{-1}$)
Buffer solution only	/	/	/	>8 h (12 % in 4 h)	/
Pristine PA	0	/	/	> 8 h (7 % in 4 h)	5.8
UiO-66(10)/PA	68.7 ± 0.8	6.3	0.15	4	9.6
UiO-66-NH_2(10)/PA	33.4 ± 0.5	6	0.15	0.5	7.4
Pristine Cotton	0	/	/	> 8 h (7 % in 4 h)	10.1
UiO-66(5)/C	47.5 ± 0.6	8.5	0.39	1h30	15.3
UiO-66-NH_2(5)/C	53.3 ± 0.8	7.4	0.33	~ 0.5	15.8

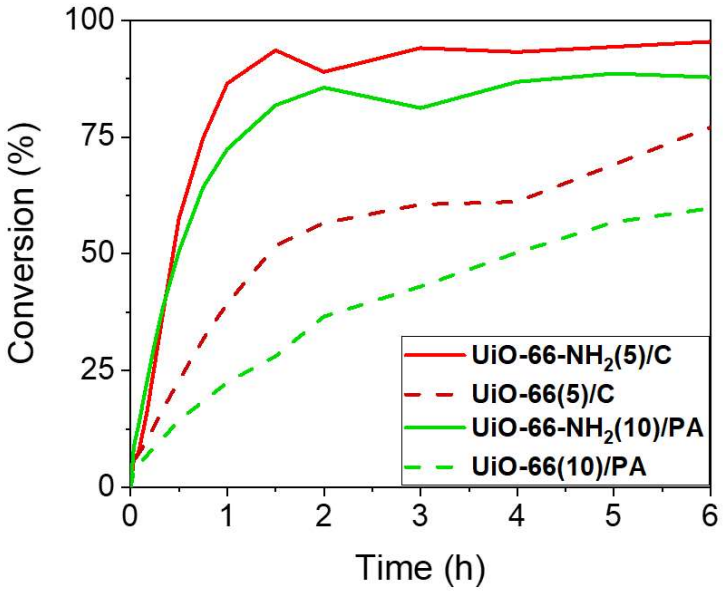

Figure 6. Kinetics of catalytic degradation of DMNP to p-nitrophenoxide using Zr-MOF composites (green: polyamide composites, red: cotton composites; full line: UiO-66-NH_2, dashed line: UiO-66).

The influence of the addition of NEM (0.5 mL) in the synthesis of UiO-66 has been studied for UiO-66(5)/C composite. Without NEM, the kinetics of the catalytic degradation of DMNP is fast, with a half-life time close to 30 min, i.e., similar to the best results presented above (Fig. S7). The detoxification of DMNP is slowed by the addition of NEM in the synthesis reaction medium, due to a deterioration of the UiO-66 structure as mentioned above. Therefore, the only beneficial contribution of the addition of NEM in the synthesis is the increase of the mechanical strength of the composite. Polyamide-based composites are therefore more interesting, being naturally more resistant to abrasion and having similar degradation efficiency than cotton composites.

These results have been compared to the ones obtained with UiO-66 or UiO-66-NH_2 composites in the literature (Table 2). The obtained half-life time of 30 min with our composites containing UiO-66-NH_2 is very short considering the low amount of MOF deposited (between 6 and 8.5 wt %). Also, our molar ratio MOF/DMNP is rather low (0.15-0.39 mol %) compared to the 6 mol % generally mentioned in the literature.[26,33] Interestingly, these low values still allow an efficient degradation of DMNP. A majority of the studies with half-life times under 30 min are obtained with higher amount of MOF (at least 15 wt %) and/or higher specific surface area. The problem is that some of these samples are obtained by using expensive methods like atomic layer deposition (ALD), making the overall process hard to scale up.[25,37] Others very promising results were obtained with MOF-808 composites combined with branched polyethyleimine BPEI, but these studies do not mention the abrasion resistance of the composites.[26,54]

Table 2. DMNP degradation efficiency comparison using UiO-66 or UiO-66-NH_2 composites from literature and our work (DMNP: between 20 and 30 µmol).

Samples	SSA (m^2/g)	% wt MOF	DMNP degradation ($t_{1/2}$ or hydrolysis rate k)	Ref
Cotton/UiO-66-NH_2	75 to 103	7.5 %	$t_{1/2}$ ~ 50 min	[55]
PA-66/UiO-66	35	20 %	k: ~5 (mM/sec x 10^{-6}) (DMNP : 0.125 µmol)	[56]
PA-66/ UiO-66-NH_2	107	29 %	k: ~33 (mM/sec x 10^{-6}) (DMNP : 0.125 µmol)	[56]
PVDF/UiO-66-NH_2	225	33 %	$t_{1/2}$ =12 min	[57]
Graphene oxide/UiO-66-NH_2	305	27.7 %	$t_{1/2}$ =1.6 min *	[51]
Polyester PET/UiO-66-NH_2	95	8 %	$t_{1/2}$ =5 min	[18]
Cotton/UiO-66-NH_2	27 to 89	/	$t_{1/2}$ =4 min	[58]
PA-6/TiO_2/UiO-66	143.9	8.8	$t_{1/2}$ =135 min	[25]
PA-6/TiO_2/UiO-66-NH_2	205.9	14.7 %	$t_{1/2}$ =7.3 min	[25]
PA-6/PDA/UiO-66-NH_2	270	28.4 %	$t_{1/2}$ =0.5 min *	[33]
PMMA/$Ti(OH)_4$ /TiO_2/UiO-66-NH_2	264	41.2 %	$t_{1/2}$ =26 min	[59]
PMMA/$Ti(OH)_4$/UiO-66	185	31 %	$t_{1/2}$ =29 min	[60]
PP/ZnO/UiO-66-NH_2	211	30.7 %	$t_{1/2}$ =2.8 min	[37]
PP/ZnO/UiO-66-NH_2	145	15.1 %	$t_{1/2}$ =10 min	[34]
PP/TiO_2/UiO-66-NH_2	132	~ 14 %	$t_{1/2}$ < 5min	[61]
PAN/PDA/UiO-66-NH_2	254	56 %	$t_{1/2}$ =1.8 min (NIR)	[62]
PIM/PAN/UiO-66-NH_2	574	/	$t_{1/2}$ ~ 45 min	[63]
PA/UiO-66-NH_2**	33.4	6.3 %	$t_{1/2}$ ~ 30 min	This work
Cotton/UiO-66-NH_2***	53.3	7 %	$t_{1/2}$ ~ 30 min	This work

* SSL: Simulated Solar Light; NIR: Near Infrared irradiation; ** from UiO-66-NH_2(10)/PA: sample; *** from UiO-66-NH_2(5)/C

Uranyl cation capture

The capture of cationic uranyl (VI) species dissolved in aqueous solutions has been investigated for one given concentration of 100 ppm of U(VI). To determine the best barrier versus uranyl in liquid media, the influence of several parameters was first tested on the UiO-66(3)/C composite, i.e pH values of 3, 5 and 7, and contact times of 1 and 4 h. From this study, it appears that the maximal uranyl adsorption is obtained at pH 7 and for a contact time of 4 h (Fig. S8). These conditions have therefore been applied for the optimized composites (identical to those used for DMNP degradation tests), and the results are presented in Table 1.

From Table 1, two conclusions can be drawn. Firstly, the adsorption or uranyl cation is very similar in UiO-66 and UiO-66-NH_2 composites. This had already been observed in the literature, where an uranyl uptake q_e of 109.9 and 114.9 mg. g^{-1} were measured for UiO-66 and UiO-66-NH_2 powder respectively.[45] The enhancement which could have been expected with the presence of amino groups (from UiO-66-NH_2), being soft donor groups for actinides, is rather low when comparing two samples with similar specific surface area (UiO-66(5)/C and UiO-66-NH_2(5)/C). Secondly, the uranyl uptake capacity is favored by a factor of ~1.5 with the cotton support compared to the polyamide one. This is due to the intrinsic property of sorption of the fabric itself, the cotton having a double capacity toward uranyl trapping. Indeed, plain cotton adsorption (10.1 mg. g^{-1}) is higher than the functionalized UiO-66(10)/PA (9.6 mg. g^{-1}). The adsorption of uranyl by cotton has been associated to the occurrence of hydroxyl groups at the surface of the fiber. The addition of Zr-based MOF slightly increased the adsorption efficiency, varying from 10.1 to 15.8 mg. g^{-1} for UiO-66-NH_2(5)/C or 15.3 mg. g^{-1} for UiO-66(5)/C.

Compared to literature, these values uptake are relatively low, as UiO-66 and UiO-66-NH_2 powder uptake values are around 110 mg. g^{-1}.[45] Their combination with graphene oxide, urea

porous organic polymer or chitosan and polyvinyl alcohol for example gave even higher values (188, 278 and 316.5 mg. g^{-1} respectively).[47,48,64,65] Concerning composites of textile/MOFs, a first study used HKUST-1 on cotton to adsorb up to 241 mg. g^{-1} of U(VI), but the exact deposition conditions of HKUST-1 were not detailed by the authors (no information about surface area, XRD, mass loading, …).[66] However, data concerning the sorption properties of UiO-n deposited on fabrics are not yet documented.

Gaseous *Kr, Xe, CO_2, CH_4 capture*

Figure 7 presents the adsorption isotherms of the four gases (Kr, Xe, CO_2, CH_4) with the optimized UiO-66/C or PA and UiO-66-NH_2 / C or PA samples. For all gases, the best adsorption capacity is measured with the UiO-66(10)/PA, with 0.9 cm^3/g for Kr, 2.9 cm^3/g for Xe, 1.3 cm^3/g for CH_4 and 5.2 cm^3/g for CO_2 at 900 mmHg (or 760 mmHg for CO_2). These results reasonably agree with the order of specific surface area, as UiO-66(10)/PA (in red in Fig. 7) possess the higher one of the four selected samples (68.7 m^2/g) and UiO-66-NH_2(10)/PA (in blue in Fig. 7) the lowest (33.4 m^2/g, see Table 1). The nature of the fiber (cotton or PA) does not play any significant role in the adsorption efficiency, except for CO_2 which is slightly adsorbed (0.9 cm^3/g for cotton and 2.1 cm^3/g for PA). This gain might be correlated to interactions of CO_2 with the hydroxyl and amide functions localized at the surface of cotton and polyamide, respectively.

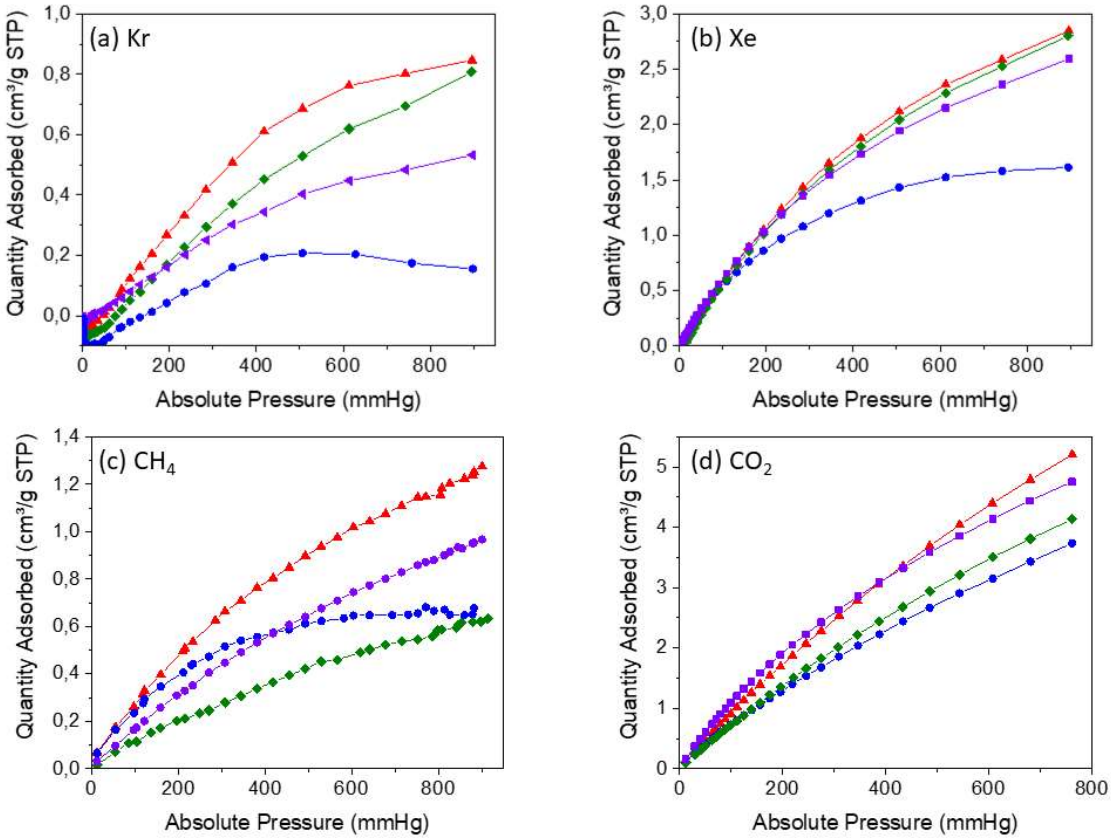

Figure 7. (a) Kr, (b) Xe, (c) CH_4 and (d) CO_2 adsorption isotherms at 20°C (red triangle: UiO-66(10)/PA; blue circles: UiO-66-NH_2(10)/PA; green diamond: UiO-66(5)/C and purple square: UiO-66-NH_2(5)/C).

To the best of our knowledge, no composite MOF/textile has been tested for gas of interest (Xe, Kr, CO_2, etc.) at room temperature in the literature. To compare our values with existing data, we have estimated the highest amount of gas uptake observed in UiO-66(10)/PA as if MOF was the only component. Knowing the percentage of MOF on this composite sample (i.e. 6.3 wt %), we therefore found adsorption uptakes of 13.5 cm^3/g for Kr, 45 cm^3/g for Xe, 20.3 cm^3/g for CH_4 and

82.5 cm^3/g for CO_2. These values are close to the ones measured with a pure UiO-66 powder, *i.e.*, 16 cm^3/g for Kr or 51 cm^3/g for Xe, or the ones found in the literature (see Table S4).[41,67,68] The small variations observed with values from literature could be due to the different temperature used for adsorption measurements (from 10 to 25 °C), as a lower temperature makes the uptake better. In the end, these close ranges of uptake capacities indicate that the deposition process on textiles did not affect the adsorptive properties of the porous UiO-66 and UiO-66-NH_2 materials.

CONCLUSION

In this study, an innovative deposition method of MOF on textile was developed using a one-pot technique by microwave-assisted synthesis. Homogeneous anchoring of well-crystallized UiO-66 and UiO-66-NH_2 particles of 60 nm size has been observed on both cotton and polyamide textiles. An easier deposition on cotton than polyamide was noted, due to more surface groups on cotton (hydroxyl especially). The quantity of UiO-66 and UiO-66-NH_2 deposited can be increased thanks to repeated coating deposition processes.

To characterize the mechanical strength of the different composites, abrasion tests have been carried out. Polyamide composites showed excellent stability regardless of the number of coating depositions. For cotton, synthesis above 90 °C with one coating deposition showed weak resistance to abrasion. This partial degradation has been attributed to acidic conditions due to HCl release during UiO-66/UiO-66-NH_2 synthesis. Therefore, we then proposed to increase the synthesis pH medium by adding basic N-ethylmorpholine (NEM). Mechanical strength of cotton composite was then increased but with a loss of UiO-66/UiO-66-NH_2 crystallinity.

In terms of CBRN (Chemical, Biological, Radiological and Nuclear) protection, two composite samples, i.e., UiO-66-NH_2(5)/C and UiO-66-NH_2(10)/PA, have shown the best results in terms of DMNP detoxification, with short half-life time of 30 min. This result highlights the ability to combine stable composite with an interesting detoxification efficiency. Due to an easier synthesis path (i.e. no NEM addition needed) and higher mechanical strength, the polyamide composites appear more promising for further researches and applications. Concerning radioactive protection, uranyl capture gave up to 15.8 mg. g^{-1} of adsorbent for the cotton-based composite UiO-66-NH_2(5)/C. At the opposite, Kr and Xe gaseous best capture efficiency were obtained with polyamide support, for the composite UiO-66(10)/PA, with 0.9 and 2.9 cm^3/g respectively. UiO-66(10)/PA also gave the best uptake for CO_2 and CH_4, with 5.2 and 1.3 cm^3/g.

ASSOCIATED CONTENT

Supporting information

The Supporting Information is available free of charge on the ACS Publications website at DOI:

Additional IR spectroscopy, abrasion tests, SEM images, XRD, catalytic degradation of DMNP, uranium uptake and comparatives tables.

AUTHOR INFORMATION

Corresponding Author

* Email address: christophe.volkringer@centralelille.fr

Author contributions

C. V planned and directed the project. N.C synthesized the materials and collected and analyzed the X-ray diffraction, SEM, BET, abrasion tests, DMNP degradation and uranium capture. M.F helped in the collection and analysis of abrasion tests. S.D helped in the collection of uranium capture experiment. N.C wrote the initial paper draft and all authors contributed to revise the paper.

Declaration of interests

The authors declare no competing financial interest.

ACKNOWLEGMENTS

This work was supported by the National Agency of Research (ANR) through the TEXMOF project (ANR-19-ASTR-0015). The authors would like to thank the AID/ DGA (Defense Innovation Agency/French Ministry of Defense) for their support. ICP analyses were performed in the « Spectrométrie par torche à plasma » platform of the Research Federation Michel-Eugène Chevreul hosted by the LASIR laboratory. The SEM national facility in Lille was supported by Conseil Régional des Hauts-de-France, European Regional Development Fund, and CNRS-INSU. The authors also thank Mr. Alexandre Fadel for his help in SEM analyses, Laurence Burylo for XRD measurements and Orfeas Plastiras for ToC artwork.

REFERENCES

(1) Dickson, E. F. G. *Personal Protective Equipment for Chemical, Biological, and Radiological Hazards: Design, Evaluation, and Selection*; John Wiley & Sons, Inc.: Hoboken, NJ, USA, 2012. https://doi.org/10.1002/9781118422991.

(2) Ormond, R. B.; Barker, R. L. Chemical, Biological, Radiological and Nuclear (CBRN) Protective Clothing. In *Protective Clothing*; Elsevier, 2014; pp 112–145. https://doi.org/10.1533/9781782420408.1.112.

(3) Dolez, P. I.; Mlynarek, J. Smart Materials for Personal Protective Equipment. In *Smart Textiles and their Applications*; Elsevier, 2016; pp 497–517. https://doi.org/10.1016/B978-0-08-100574-3.00022-9.

(4) Mao, N. High Performance Textiles for Protective Clothing. In *High Performance Textiles and their Applications*; Elsevier, 2014; pp 91–143. https://doi.org/10.1533/9780857099075.91.

(5) Bhuiyan, M. A. R.; Wang, L.; Shaid, A.; Shanks, R. A.; Ding, J. Advances and Applications of Chemical Protective Clothing System. *J. Ind. Text.* **2019**, *49* (1), 97–138. https://doi.org/10.1177/1528083718779426.

(6) Thakare, V. B.; Tripathi, N. K.; Singh, V. V.; Sathe, M.; Singh, B. Activated Carbon Fabric: An Adsorbent Material for Chemical Protective Clothing. *Def. Sci. J.* **2017**, *68* (1), 83. https://doi.org/10.14429/dsj.68.11734.

(7) Couzon, N.; Dhainaut, J.; Campagne, C.; Royer, S.; Loiseau, T.; Volkringer, C. Porous Textile Composites (PTCs) for the Removal and the Decomposition of Chemical Warfare Agents (CWAs) – A Review. *submitted* **2022**.

(8) Kaiser, R.; Kulczyk, A.; Rich, D.; Willey, R. J.; Minicucci, J.; MacIver, B. Effect of Pore Size Distribution of Commercial Activated Carbon Fabrics on the Adsorption of CWA Simulants from the Liquid Phase. *Ind. Eng. Chem. Res.* **2007**, *46* (19), 6126–6132. https://doi.org/10.1021/ie061429n.

(9) Hudiono, Y. C.; Miller, A. L.; Gibson, P. W.; LaFrate, A. L.; Noble, R. D.; Gin, D. L. A Highly Breathable Organic/Inorganic Barrier Material That Blocks the Passage of Mustard Agent Simulants. *Ind. Eng. Chem. Res.* **2012**, *51* (21), 7453–7456. https://doi.org/10.1021/ie202977e.

(10) Wagner, G. W.; Bartram, P. W. Reactions of VX, HD, and Their Simulants with NaY and AgY Zeolites. Desulfurization of VX on AgY. *Langmuir* **1999**, *15* (23), 8113–8118. https://doi.org/10.1021/la990716b.

(11) McEntee, M.; Gordon, W. O.; Balboa, A.; Delia, D. J.; Pitman, C. L.; Pennington, A. M.; Rolison, D. R.; Pietron, J. J.; DeSario, P. A. Mesoporous Copper Nanoparticle/TiO_2 Aerogels for Room-Temperature Hydrolytic Decomposition of the Chemical Warfare Simulant Dimethyl Methylphosphonate. *ACS Appl. Nano Mater.* **2020**, *3* (4), 3503–3512. https://doi.org/10.1021/acsanm.0c00228.

(12) Štengl, V.; Králová, D.; Opluštil, F.; Němec, T. Mesoporous Manganese Oxide for Warfare Agents Degradation. *Microporous Mesoporous Mater.* **2012**, *156*, 224–232. https://doi.org/10.1016/j.micromeso.2012.02.031.

(13) Islamoglu, T.; Chen, Z.; Wasson, M. C.; Buru, C. T.; Kirlikovali, K. O.; Afrin, U.; Mian, M. R.; Farha, O. K. Metal–Organic Frameworks against Toxic Chemicals. *Chem. Rev.* **2020**, acs.chemrev.9b00828. https://doi.org/10.1021/acs.chemrev.9b00828.

(14) Katz, M. J.; Mondloch, J. E.; Totten, R. K.; Park, J. K.; Nguyen, S. T.; Farha, O. K.; Hupp, J. T. Simple and Compelling Biomimetic Metal-Organic Framework Catalyst for the Degradation of Nerve Agent Simulants. *Angew. Chem.* **2014**, *126* (2), 507–511. https://doi.org/10.1002/ange.201307520.

(15) Grissom, T. G.; Plonka, A. M.; Sharp, C. H.; Ebrahim, A. M.; Tian, Y.; Collins-Wildman, D. L.; Kaledin, A. L.; Siegal, H. J.; Troya, D.; Hill, C. L.; Frenkel, A. I.; Musaev, D. G.; Gordon, W. O.; Karwacki, C. J.; Mitchell, M. B.; Morris, J. R. Metal−Organic Framework- and Polyoxometalate-Based Sorbents for the Uptake and Destruction of Chemical Warfare Agents. *ACS Appl. Mater. Interfaces* **2021**, *12*, 14641–14661.

(16) Peterson, G. W.; Moon, S.-Y.; Wagner, G. W.; Hall, M. G.; DeCoste, J. B.; Hupp, J. T.; Farha, O. K. Tailoring the Pore Size and Functionality of UiO-Type Metal−Organic Frameworks for Optimal Nerve Agent Destruction. *Inorg. Chem.* **2015**, *54*, 9684–9686.

(17) Chen, Z.; Ma, K.; Mahle, J. J.; Wang, H.; Syed, Z. H.; Atilgan, A.; Chen, Y.; Xin, J. H.; Islamoglu, T.; Peterson, G. W.; Farha, O. K. Integration of Metal–Organic Frameworks on Protective Layers for Destruction of Nerve Agents under Relevant Conditions. *J. Am. Chem. Soc.* **2019**, *141* (51), 20016–20021. https://doi.org/10.1021/jacs.9b11172.

(18) Ma, K.; Islamoglu, T.; Chen, Z.; Li, P.; Wasson, M. C.; Chen, Y.; Wang, Y.; Peterson, G. W.; Xin, J. H.; Farha, O. K. Scalable and Template-Free Aqueous Synthesis of Zirconium-Based Metal–Organic Framework Coating on Textile Fiber. *J. Am. Chem. Soc.* **2019**, *141* (39), 15626–15633. https://doi.org/10.1021/jacs.9b07301.

(19) Palomba, J. M.; Credille, C. V.; Kalaj, M.; DeCoste, J. B.; Peterson, G. W.; Tovar, T. M.; Cohen, S. M. High-Throughput Screening of Solid-State Catalysts for Nerve Agent

Degradation. *Chem. Commun.* **2018**, *54* (45), 5768–5771. https://doi.org/10.1039/C8CC03255F.

(20) Ploskonka, A. M.; DeCoste, J. B. Insight into Organophosphate Chemical Warfare Agent Simulant Hydrolysis in Metal-Organic Frameworks. *J. Hazard. Mater.* **2019**, *375*, 191–197. https://doi.org/10.1016/j.jhazmat.2019.04.044.

(21) Barton, H. F.; Jamir, J. D.; Davis, A. K.; Peterson, G. W.; Parsons, G. N. Doubly-Protective MOF-Photo-Fabrics: Facile Template-Free Synthesis of PCN-222-Textiles Enables Rapid Hydrolysis, Photo-Hydrolysis and Selective Oxidation of Multiple Chemical Warfare Agents and Simulants. *Chem Eur J* **2020**, *26*. https://doi.org/10.1002/chem.202003716.

(22) Liu, Y.; Howarth, A. J.; Vermeulen, N. A.; Moon, S.-Y.; Hupp, J. T.; Farha, O. K. Catalytic Degradation of Chemical Warfare Agents and Their Simulants by Metal-Organic Frameworks. *Coord. Chem. Rev.* **2017**, *346*, 101–111. https://doi.org/10.1016/j.ccr.2016.11.008.

(23) Islamoglu, T.; Ortuño, M. A.; Proussaloglou, E.; Howarth, A. J.; Vermeulen, N. A.; Atilgan, A.; Asiri, A. M.; Cramer, C. J.; Farha, O. K. Presence versus Proximity: The Role of Pendant Amines in the Catalytic Hydrolysis of a Nerve Agent Simulant. *Angew. Chem. Int. Ed.* **2018**, *57* (7), 1949–1953. https://doi.org/10.1002/anie.201712645.

(24) Moon, S.-Y.; Liu, Y.; Hupp, J. T.; Farha, O. K. Instantaneous Hydrolysis of Nerve-Agent Simulants with a Six-Connected Zirconium-Based Metal-Organic Framework. *Angew. Chem. Int. Ed.* **2015**, *54* (23), 6795–6799. https://doi.org/10.1002/anie.201502155.

(25) Zhao, J.; Lee, D. T.; Yaga, R. W.; Hall, M. G.; Barton, H. F.; Woodward, I. R.; Oldham, C. J.; Walls, H. J.; Peterson, G. W.; Parsons, G. N. Ultra-Fast Degradation of Chemical Warfare

Agents Using MOF-Nanofiber Kebabs. *Angew. Chem. Int. Ed.* **2016**, *55* (42), 13224–13228. https://doi.org/10.1002/anie.201606656.

(26) Ma, K.; Wasson, M. C.; Wang, X.; Zhang, X.; Idrees, K. B.; Chen, Z.; Wu, Y.; Lee, S.-J.; Cao, R.; Chen, Y.; Yang, L.; Son, F. A.; Islamoglu, T.; Peterson, G. W.; Mahle, J. J.; Farha, O. K. Near-Instantaneous Catalytic Hydrolysis of Organophosphorus Nerve Agents with Zirconium-Based MOF/Hydrogel Composites. *Chem Catal.* **2021**, *1* (3), 721–733. https://doi.org/10.1016/j.checat.2021.06.008.

(27) Giannakoudakis, D. A.; Hu, Y.; Florent, M.; Bandosz, T. J. Smart Textiles of MOF/g-C_3N_4 Nanospheres for the Rapid Detection/Detoxification of Chemical Warfare Agents. *Nanoscale Horiz* **2017**, *2* (6), 356–364. https://doi.org/10.1039/C7NH00081B.

(28) Laurila, E.; Thunberg, J.; Argent, S. P.; Champness, N. R.; Zacharias, S.; Westman, G.; Öhrström, L. Enhanced Synthesis of Metal-Organic Frameworks on the Surface of Electrospun Cellulose Nanofibers: Enhanced Synthesis of Metal-Organic Frameworks. *Adv. Eng. Mater.* **2015**, *17* (9), 1282–1286. https://doi.org/10.1002/adem.201400565.

(29) Peterson, G. W.; Lee, D. T.; Barton, H. F.; Epps, T. H.; Parsons, G. N. Fibre-Based Composites from the Integration of Metal–Organic Frameworks and Polymers. *Nat. Rev. Mater.* **2021**, *6* (7), 605–621. https://doi.org/10.1038/s41578-021-00291-2.

(30) Dou, Y.; Zhang, W.; Kaiser, A. Electrospinning of Metal–Organic Frameworks for Energy and Environmental Applications. *Adv. Sci.* **2020**, *7* (3), 1902590. https://doi.org/10.1002/advs.201902590.

(31) Rubin, H. N.; Neufeld, B. H.; Reynolds, M. M. Surface-Anchored Metal–Organic Framework–Cotton Material for Tunable Antibacterial Copper Delivery. *ACS Appl. Mater. Interfaces* **2018**, *10* (17), 15189–15199. https://doi.org/10.1021/acsami.7b19455.

(32) Lu, L.; Hu, C.; Zhu, Y.; Zhang, H.; Li, R.; Xing, Y. Multi-Functional Finishing of Cotton Fabrics by Water-Based Layer-by-Layer Assembly of Metal–Organic Framework. *Cellulose* **2018**, *25* (7), 4223–4238. https://doi.org/10.1007/s10570-018-1838-8.

(33) Yao, A.; Jiao, X.; Chen, D.; Li, C. Bio-Inspired Polydopamine-Mediated Zr-MOF Fabrics for Solar Photothermal-Driven Instantaneous Detoxification of Chemical Warfare Agent Simulants. *ACS Appl. Mater. Interfaces* **2020**, *12* (16), 18437–18445. https://doi.org/10.1021/acsami.9b22242.

(34) Lee, D. T.; Zhao, J.; Oldham, C. J.; Peterson, G. W.; Parsons, G. N. UiO-66-NH $_2$ Metal–Organic Framework (MOF) Nucleation on TiO_2, ZnO, and Al_2O_3 Atomic Layer Deposition-Treated Polymer Fibers: Role of Metal Oxide on MOF Growth and Catalytic Hydrolysis of Chemical Warfare Agent Simulants. *ACS Appl. Mater. Interfaces* **2017**, *9* (51), 44847–44855. https://doi.org/10.1021/acsami.7b15397.

(35) Zhao, J.; Losego, M. D.; Lemaire, P. C.; Williams, P. S.; Gong, B.; Atanasov, S. E.; Blevins, T. M.; Oldham, C. J.; Walls, H. J.; Shepherd, S. D.; Browe, M. A.; Peterson, G. W.; Parsons, G. N. Highly Adsorptive, MOF-Functionalized Nonwoven Fiber Mats for Hazardous Gas Capture Enabled by Atomic Layer Deposition. *Adv. Mater. Interfaces* **2014**, *1* (4), 1400040. https://doi.org/10.1002/admi.201400040.

(36) Kalaj, M.; Cohen, S. M. Spray-Coating of Catalytically Active MOF–Polythiourea through Postsynthetic Polymerization. *Angew. Chem. Int. Ed.* **2020**, *59* (33), 13984–13989. https://doi.org/10.1002/anie.202004205.

(37) Lee, D. T.; Zhao, J.; Peterson, G. W.; Parsons, G. N. Catalytic “MOF-Cloth” Formed via Directed Supramolecular Assembly of UiO-66-NH $_2$ Crystals on Atomic Layer Deposition-

Coated Textiles for Rapid Degradation of Chemical Warfare Agent Simulants. *Chem. Mater.* **2017**, *29* (11), 4894–4903. https://doi.org/10.1021/acs.chemmater.7b00949.

(38) Centrone, A.; Yang, Y.; Speakman, S.; Bromberg, L.; Rutledge, G. C.; Hatton, T. A. Growth of Metal−Organic Frameworks on Polymer Surfaces. *J. Am. Chem. Soc.* **2010**, *132* (44), 15687–15691. https://doi.org/10.1021/ja106381x.

(39) Liu, C.; Wu, Y.; Morlay, C.; Gu, Y.; Gebremariam, B.; Yuan, X.; Li, F. General Deposition of Metal−Organic Frameworks on Highly Adaptive Organic−Inorganic Hybrid Electrospun Fibrous Substrates. *ACS Appl. Mater. Interfaces* **2016**, *8*, 2552–2561.

(40) Rubio-Martinez, M.; Avci-Camur, C.; Thornton, A. W.; Imaz, I.; Maspoch, D.; Hill, M. R. New Synthetic Routes towards MOF Production at Scale. *Chem. Soc. Rev.* **2017**, *46* (11), 3453–3480. https://doi.org/10.1039/C7CS00109F.

(41) Lee, S.-J.; Kim, S.; Kim, E.-J.; Kim, M.; Bae, Y.-S. Adsorptive Separation of Xenon/Krypton Mixtures Using Ligand Controls in a Zirconium-Based Metal-Organic Framework. *Chem. Eng. J.* **2018**, *335*, 345–351. https://doi.org/10.1016/j.cej.2017.10.155.

(42) Zhang, H.; Liu, W.; Li, A.; Zhang, D.; Li, X.; Zhai, F.; Chen, L.; Chen, L.; Wang, Y.; Wang, S. Three Mechanisms in One Material: Uranium Capture by a Polyoxometalate–Organic Framework through Combined Complexation, Chemical Reduction, and Photocatalytic Reduction. *Angew Chem Int Ed* **2019**, *58* (16110–16114), 5.

(43) Wang, Y.; Liu, W.; Bai, Z.; Zheng, T.; Silver, M. A.; Li, Y.; Wang, Y.; Wang, X.; Diwu, J.; Chai, Z.; Wang, S. Employing an Unsaturated Th4+ Site in a Porous Thorium–Organic Framework for Kr/Xe Uptake and Separation. *Angew Chem Int Ed* **2018**, *57* (5783–5787), 5.

(44) Zheng, T.; Yang, Z.; Gui, D.; Liu, Z.; Wang, X.; Dai, X.; Liu, S.; Zhang, L.; Gao, Y.; Chen, L.; Sheng, D.; Wang, Y.; Diwu, J.; Wang, J.; Zhou, R.; Chai, Z.; Albrecht-Schmitt, T. E.;

Wang, S. Overcoming the Crystallization and Designability Issues in the Ultrastable Zirconium Phosphonate Framework System. *Nat. Commun.* **2017**, *8* (15369), 11.

(45) Luo, B.-C.; Yuan, L.-Y.; Chai, Z.-F.; Shi, W.-Q.; Tang, Q. U(VI) Capture from Aqueous Solution by Highly Porous and Stable MOFs: UiO-66 and Its Amine Derivative. *J. Radioanal. Nucl. Chem.* **2016**, *307* (1), 269–276. https://doi.org/10.1007/s10967-015-4108-3.

(46) ISO; NF EN ISO 12947-3. *Determination of the Abrasion Resistance of Fabrics by the Martindale Method. Part 3: Determination of Mass Loss*; 1999.

(47) Fotovat, H.; Khajeh, M.; Oveisi, A. R.; Ghaffari-Moghaddam, M.; Daliran, S. A Hybrid Material Composed of an Amino-Functionalized Zirconium-Based Metal-Organic Framework and a Urea-Based Porous Organic Polymer as an Efficient Sorbent for Extraction of Uranium(VI). *Microchim. Acta* **2018**, *185* (10), 469. https://doi.org/10.1007/s00604-018-2991-3.

(48) Yang, P.; Liu, Q.; Liu, J.; Zhang, H.; Li, Z.; Li, R.; Liu, L.; Wang, J. Interfacial Growth of a Metal–Organic Framework (UiO-66) on Functionalized Graphene Oxide (GO) as a Suitable Seawater Adsorbent for Extraction of Uranium(VI). *J. Mater. Chem. A* **2017**, *5* (34), 17933–17942. https://doi.org/10.1039/C6TA10022H.

(49) Xu, W.; Dong, M.; Di, L.; Zhang, X. A Facile Method for Preparing UiO-66 Encapsulated Ru Catalyst and Its Application in Plasma-Assisted CO2 Methanation. *Nanomaterials* **2019**, *9* (10), 1432. https://doi.org/10.3390/nano9101432.

(50) Valenzano, L.; Civalleri, B.; Chavan, S.; Bordiga, S.; Nilsen, M. H.; Jakobsen, S.; Lillerud, K. P.; Lamberti, C. Disclosing the Complex Structure of UiO-66 Metal Organic Framework:

A Synergic Combination of Experiment and Theory. *Chem. Mater.* **2011**, *23* (7), 1700–1718. https://doi.org/10.1021/cm1022882.

(51) Song, L.; Zhao, T.; Yang, D.; Wang, X.; Hao, X.; Liu, Y.; Zhang, S.; Yu, Z.-Z. Photothermal Graphene/UiO-66-NH2 Fabrics for Ultrafast Catalytic Degradation of Chemical Warfare Agent Simulants. *J. Hazard. Mater.* **2020**, *393*, 122332. https://doi.org/10.1016/j.jhazmat.2020.122332.

(52) Kirlikovali, K. O.; Chen, Z.; Islamoglu, T.; Hupp, J. T.; Farha, O. K. Zirconium-Based Metal–Organic Frameworks for the Catalytic Hydrolysis of Organophosphorus Nerve Agents. *ACS Appl. Mater. Interfaces* **2020**, *12* (13), 14702–14720. https://doi.org/10.1021/acsami.9b20154.

(53) Katz, M. J.; Moon, S.-Y.; Mondloch, J. E.; Beyzavi, M. H.; Stephenson, C. J.; Hupp, J. T.; Farha, O. K. Exploiting Parameter Space in MOFs: A 20-Fold Enhancement of Phosphate-Ester Hydrolysis with UiO-66-NH_2. *Chem. Sci.* **2015**, *6* (4), 2286–2291. https://doi.org/10.1039/C4SC03613A.

(54) Cheung, Y. H.; Ma, K.; Wasson, M. C.; Wang, X.; Idrees, K. B.; Islamoglu, T.; Mahle, J.; Peterson, G. W.; Xin, J. H.; Farha, O. K. Environmentally Benign Biosynthesis of Hierarchical MOF/Bacterial Cellulose Composite Sponge for Nerve Agent Protection. **2022**, 8. https://doi.org/10.1002/anie.202202207.

(55) Bunge, M. A.; Davis, A. B.; West, K. N.; West, C. W.; Glover, T. G. Synthesis and Characterization of UiO-66-NH_2 Metal–Organic Framework Cotton Composite Textiles. *Ind. Eng. Chem. Res.* **2018**, *57* (28), 9151–9161. https://doi.org/10.1021/acs.iecr.8b01010.

(56) Kalaj, M.; Denny, M. S.; Bentz, K. C.; Palomba, J. M.; Cohen, S. M. Nylon–MOF Composites through Postsynthetic Polymerization. *Angew. Chem. Int. Ed.* **2019**, *58* (8), 2336–2340. https://doi.org/10.1002/anie.201812655.

(57) Lu, A. X.; McEntee, M.; Browe, M. A.; Hall, M. G.; DeCoste, J. B.; Peterson, G. W. MOFabric: Electrospun Nanofiber Mats from PVDF/UiO-66-NH_2 for Chemical Protection and Decontamination. *ACS Appl. Mater. Interfaces* **2017**, *9* (15), 13632–13636. https://doi.org/10.1021/acsami.7b01621.

(58) Bunge, M. A.; Pasciak, E.; Choi, J.; Haverhals, L.; Reichert, W. M.; Glover, T. G. Ionic Liquid Welding of the UIO-66-NH_2 MOF to Cotton Textiles. *Ind. Eng. Chem. Res.* **2020**, *59* (43), 19285–19298. https://doi.org/10.1021/acs.iecr.0c03763.

(59) Dwyer, D. B.; Lee, D. T.; Boyer, S.; Bernier, W. E.; Parsons, G. N.; Jones, W. E. Toxic Organophosphate Hydrolysis Using Nanofiber-Templated UiO-66-NH_2 Metal–Organic Framework Polycrystalline Cylinders. *ACS Appl. Mater. Interfaces* **2018**, *10* (30), 25794–25803. https://doi.org/10.1021/acsami.8b08167.

(60) McCarthy, D. L.; Liu, J.; Dwyer, D. B.; Troiano, J. L.; Boyer, S. M.; DeCoste, J. B.; Bernier, W. E.; Jones, Jr, W. E. Electrospun Metal–Organic Framework Polymer Composites for the Catalytic Degradation of Methyl Paraoxon. *New J. Chem.* **2017**, *41* (17), 8748–8753. https://doi.org/10.1039/C7NJ00525C.

(61) Lee, D. T.; Dai, Z.; Peterson, G. W.; Hall, M. G.; Pomerantz, N. L.; Hoffman, N.; Parsons, G. N. Highly Breathable Chemically-Protective MOF-Fiber Catalysts. *Adv. Funct. Mater.* **2021**, 2108004. https://doi.org/10.1002/adfm.202108004.

(62) Yao, A.; Jiao, X.; Chen, D.; Li, C. Photothermally Enhanced Detoxification of Chemical Warfare Agent Simulants Using Bioinspired Core–Shell Dopamine–Melanin@Metal–

Organic Frameworks and Their Fabrics. *ACS Appl. Mater. Interfaces* **2019**, *11* (8), 7927–7935. https://doi.org/10.1021/acsami.8b19445.

(63) Wang, S.; Pomerantz, N. L.; Dai, Z.; Xie, W.; Anderson, E. E.; Miller, T.; Khan, S. A.; Parsons, G. N. Polymer of Intrinsic Microporosity (PIM) Based Fibrous Mat: Combining Particle Filtration and Rapid Catalytic Hydrolysis of Chemical Warfare Agent Simulants into a Highly Sorptive, Breathable, and Mechanically Robust Fiber Matrix. *Mater. Today Adv.* **2020**, *8*, 100085. https://doi.org/10.1016/j.mtadv.2020.100085.

(64) Wang, Y.; Long, J.; Xu, W.; Luo, H.; Liu, J.; Zhang, Y.; Li, J.; Luo, X. Removal of Uranium(VI) from Simulated Wastewater by a Novel Porous Membrane Based on Crosslinked Chitosan, UiO-66-NH2 and Polyvinyl Alcohol. *J. Radioanal. Nucl. Chem.* **2021**, *328* (1), 397–410. https://doi.org/10.1007/s10967-021-07649-4.

(65) Zhao, Z.; Cheng, G.; Zhang, Y.; Han, B.; Wang, X. Metal-Organic-Framework Based Functional Materials for Uranium Recovery: Performance Optimization and Structure/Functionality-Activity Relationships. *ChemPlusChem* **2021**, *86* (8), 1177–1192. https://doi.org/10.1002/cplu.202100315.

(66) Yang, A.; Wang, Z.; Zhu, Y. Facile Preparation and Adsorption Performance of Low-Cost MOF@cotton Fibre Composite for Uranium Removal. *Sci. Rep.* **2020**, *10* (1), 19271. https://doi.org/10.1038/s41598-020-76173-4.

(67) Huang, A.; Wan, L.; Caro, J. Microwave-Assisted Synthesis of Well-Shaped UiO-66-NH_2 with High CO_2 Adsorption Capacity. *Mater. Res. Bull.* **2018**, *98*, 308–313. https://doi.org/10.1016/j.materresbull.2017.10.038.

(68) Xian, S.; Wu, Y.; Wu, J.; Wang, X.; Xiao, J. Enhanced Dynamic CO_2 Adsorption Capacity and CO_2/CH_4 Selectivity on Polyethylenimine-Impregnated UiO-66. *Ind. Eng. Chem. Res.* **2015**, *54* (44), 11151–11158. https://doi.org/10.1021/acs.iecr.5b03517.

Table of Contents (TOC):